Effect of Calcination Temperature on the Photocatalytic H_2 Evolution of Bronze Phase Monoclinic TiO_2(B) Nanosheets

[1]Min Xu, [2]Muhammad Shakeel Khan, [3]Perveen Fazil*, [2]Muhammad Ateeq**
[1]College of Science & Technology, Ningbo University, Ningbo 315300, P. R. China.
[2]Department of Chemistry, Abdul Wali Khan University Mardan, 23200, Pakistan.
[3]Department of Chemistry, University of Karachi, Karachi-75270, Pakistan.
m.ateeq@awkum.edu.pk*

(Received on 16th Nov 2021, accepted in revised form 29th December 2021)

Summary: In this work, we have successfully fabricated bronze phase monoclinic TiO_2 (B) nanosheets from $TiCl_3$ under hydrothermal conditions. The fabricated samples were calcined at different annealing temperature (100, 200, 300, 400 and 500 °C) to select optimum temperature under UV light irradiation for the efficient photocatalytic water splitting. Different techniques were used for the characterization of fabricated photocatalysts. Interestingly, the sample calcined at 400 °C delivered optimum H_2 evolution from water which is attributed to the relatively high surface area and effective charge separation. The characteristic anisotropic nature of TiO_2(B) plays very crucial role in charge separation which is evident from photoluminescence spectra, steady-state surface photovoltage spectra, and produced hydroxyl radical amount. It has been concluded that optimum annealing temperature generally introduces charge trapping centres which help in the separation of excite charges for improved photocatalytic activity. However, high temperature results in particles aggregation to reduce the surface area and hence retards the photocatalytic efficiency. This work will direct future research to fabricate materials at optimized temperature for the improved photocatalytic activities.

Keywords: Monoclinic TiO_2(B); annealing temperature; H_2 evolution; charge trapping centres; hydroxyl radical

Introduction

Environmental pollution and energy crises have shaped massive research attraction to cope with these problems. Especially, the rapid depletion of hydrocarbon fuels has forced the world to think about renewable energy sources [1-9]. An everlasting solution was provided by photocatalysis to receive the shower of solar energy photons and store their energies in the chemical bonds of certain molecules. The storage of solar energy in the chemical bonds of H_2 molecules is a feasible and environment friendly technique and can be generated by splitting the plenty available water molecules photocatalytically [10-20]. This process of photocatalysis, therefore, requires the presence of a suitable photocatalyst to produce the required results.

TiO_2 is the first generation photocatalyst and has shown remarkable photocatalytic activities in water splitting, carbon dioxide conversion, pollutants degradation, N_2 conversion, organic synthesis and bacterial inactivation [21-29]. It is available in a number of polymorphic forms. The most important amongst them include bronze phase monoclinic TiO_2(B), TiO_2(H), brookite (orthorhombic), anatase (tetragonal), rutile (tetragonal), and TiO_2(R). Amongst the known polymorphs, monoclinic TiO_2(B) has attracted massive research recently [30-37]. Compare to other polymorphs, TiO_2(B) possesses more open channels in its crystal lattice which play important role in photocatalysis. Its stability is low and requires harsh conditions for preparation. It shows typical pseudocapacitive character and therefore is used as anode materials in electrolytic cells and lithium-ion battery. Its density is minimal compare to other polymorphs [38-40]. Its band gap is nearly equal to the band gap of anatase form. However, its distinctive structure with anisotropic characters also shows some potential application in dye sensitized solar cells, supercapacitors and smart windows photocatalytic water splitting and pollutants degradation. Its anisotropic character plays very crucial role in photocatalysis as the excited charges could move in different directions along the anisotropic structure to improve charge separation for extended photocatalytic activity. Since it is a metastable monoclinic phase of TiO_2, the higher annealing temperature transfers it to anatase phase and this conversion is completed up to 700 °C [41, 42]. At present, monoclinic TiO_2(B) has been synthesized in different morphologies such as nanowires and nanotubes possessing high surface area with remarkable photocatalytic activity [43].

Calcination temperature broadly controls the nature and photocatalytic activities of these different polymorphs. Therefore, understanding the effect of calcination temperature is very crucial as it helps to control the size and growth of particles and influences the photocatalytic activity [44-47]. Moreover, optimum annealing temperature generally introduces charge trapping centres which help in the separation of excite

***To whom all correspondence should be addressed.**

charges for improved photocatalytic activity. Also, high temperature results in particles aggregation to reduce the surface area and hence retards the photocatalytic efficiency.

This study is concerned with the synthesis of bronze phase monoclinic TiO_2(B) nanosheets and the calcination temperature effect on the structure and photocatalytic activity of TiO_2(B) for H_2 evolution from water under solar light irradiation. Monoclinic TiO_2(B) nanosheets were fabricated from $TiCl_3$ under hydrothermal conditions and the samples were calcined at different annealing temperature (100, 200, 300, 400 and 500 ºC) to select optimum temperature under UV light irradiation for the efficient photocatalytic water splitting. Interestingly, the sample calcined at 400 ºC delivered optimum H_2 evolution from water which is due to the enhanced surface area and effective charge separation. We hope that this work will direct future research to fabricate materials at optimized temperature for the improved photocatalytic activities.

Experimental

Monoclinic TiO_2(B) nanosheets were prepared hydrothermally from $TiCl_3$. In a typical experiment, 5 ml $TiCl_3$ were diluted with 15% V/W aqueous HCl solution and mixed with 75 ml ethylene glycol to form a homogeneous mixture. The hydrothermal heating was conducted at 200 ºC in a Teflon autoclave (100 mL) for 1 h and precipitate obtained was separated and washed several times with ethanol and deionized water to remove the impurities such as organic and inorganic. The white precipitate was dried overnight in an oven and then calcined at different temperatures (100, 200, 300, 400 and 500 ºC) for two hours in N_2 atmosphere to get monoclinic TiO_2(B) nanosheets. The synthesized samples were represented by TiO_2-X where X shows the calcination temperature of the samples.

Characterization techniques

The crystal structure of these fabricated samples were determined by X-rays D8 Advance diffractometer made by Bruker containing graphitic monochromatized Cu Kα radiator. The morphological study was conducted with help of transmission electron microscopic (JEOL JEM-2100) with operational voltage of 200 kV. The light absorption capacity of the fabricated samples was determined by taking their ultraviolet-visible diffuse reflectance spectra with Shimadzu UV-2550 spectrometer applying $BaSO_4$ as a reference material. The photoluminescence (PL) spectra were conducted with help of (Perkin-Elmer LS55 spectrofluoro-photometer at 265 nm excitation wavelength. The steady-state surface photovoltage spectra (SS-SPS) were conducted in controlled atmosphere applying a homemade built equipment carrying a lock-in amplifier (SR830) and a light chopper (SR540). The prepared samples were first crammed between two indium tin oxide (ITO) glass electrodes placed in an atmosphere controlled closed container and then irradiated with a 500W Xe lamp (CHF XQ500W, Global Xe lamp power). The radiations were first passed through a double prism monochromator (SBP300) to obtain a monochromatic radiation and then target on the sample for the measurement of the steady-state surface photovoltage spectra.

Measurement of •OH radicals

The quantity of •OH radicals formed by different photocatalysts was calculated with coumarin solution test. About 50 mL coumarin solution (0.001 M) was mixed with photocatalyst (0.05 g) under vigorous stirring for an hour and kept in dark to adsorb maximum amount of coumarin on photocatalyst surface. The mixture was then irradiated with a 150 W Xe lamp for 60 min. About 5 ml sample was collected for the fluorescence spectrum, which was recorded on Perkin-Elmer LS55 spectrofluoro-photometer. The 7-hydroxycoumarin was excited at 390 nm and emission spectrum was recorded at 460 nm.

Photocatalytic activities

The fabricated samples obtained at different temperatures were then subjected to photocatalytic activities under UV solar light irradiation for H_2 generation from water. The amount of H_2 produced was determined on Perfect light, Beijing, Lab Solar III which is a hydrogen production system. About 0.1 g sample was dispersed in a solution containing 80 ml deionized water and 20 ml methanol as hole scavenger in a reaction cell under vigorous stirring. Before irradiation, the dispersion was stirred in dark for an hour to adsorb water molecules on the surface of the photocatalyst and deaerated the instrument to eradicate gases dissolved in water. After that, the sample was irradiated with a 300 W Xe lamp under UV solar light and the produced H_2 was investigated by an inline gas chromatograph (7900, TCD, molecular sieve 5 Å, N_2 carrier, Tec comp.).

Results and Discussion

The X-ray diffractometric (XRD) data of the samples prepared under different calcination temperatures is given in Fig 1A. It is clear that all samples prepared at high temperature show characteristic peaks of TiO_2 [48]. The XRD peaks at 14.27, 24.98, 28.81 and 33.34º appeared in the case of TiO_2-100 and TiO_2-200 prepared at lower temperature are relatively broad and

lower in intensities indicating incomplete crystallization. When temperature is increased, the crystalinity is gradually improved as shown by the XRD peaks at 14.27, 24.98, 28.81, 33.34, 43.69, 48.54 and 58.4° corresponded respectively to the (001), (110), (002), (310), (003), (020) and (-421) crystal lattice planes of monoclinic TiO_2. At still higher temperature, an XRD peak appears at 62.3 related to anatase TiO_2 [49, 50]. Interestingly, these XRD peaks are grown in intensities and become sharp as temperature is increased. This is because, the size confinement introduces intrinsic strain and other essential defects during fabrication process. Thus, the crystallinity of monoclinic TiO_2(B) nanosheets increases with temperature which has a direct effect on the photocatalytic activity.

The light absorption capacity of the samples was checked by taking their UV-vis absorption spectra and the results are shown in Fig 1B. Obviously, all the samples show absorption edges in UV region. The samples TiO_2-100 and TiO_2-200 prepared at relatively low calcination temperature show weak absorption spectra at around 340 nm showing a band gap of 3.64 eV. As calcination temperature is increased, the light absorption of the samples is increased. Obviously, all the three samples calcined at higher temperature (TiO_2-300 and TiO_2-400 and TiO_2-500) show that the absorption edges are slightly blue shifted which is related to the decreased particle size because of the quantum confinement effect.

The Scanning electron microscopy (SEM) and transmission electron microscopy (TEM) images of the samples calcined at 400 and 500 ºC are given in Fig 2. As can be seen from SEM images in Fig 2A and 2B, the nanosheet like TiO_2(B) particles are homogeneously distributed. The TEM image of monoclinic TiO_2(B) confirms the nanosheets like hierarchical structure (Fig 2C). The HRTEM image in Fig 2D shows lattice fringes related to and (110) crystal plane of TiO_2(B) with d-spacing of 0.35 nm.

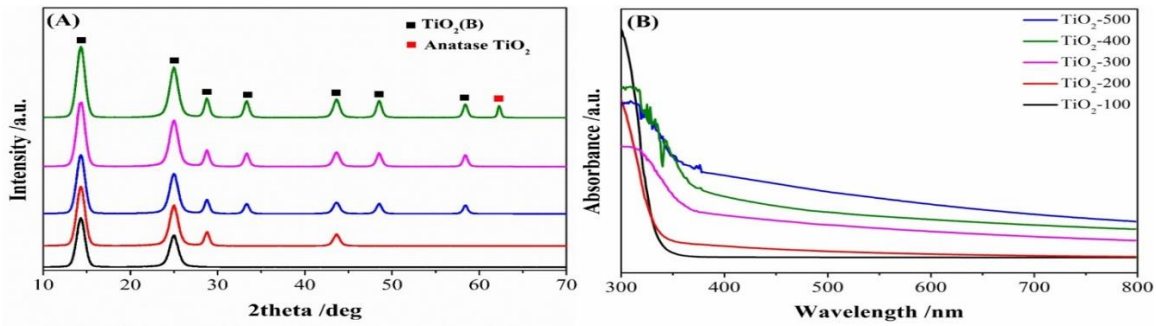

Fig 1: XRD patterns (A) and UV-Vis absorption spectra of TiO_2-X (B).

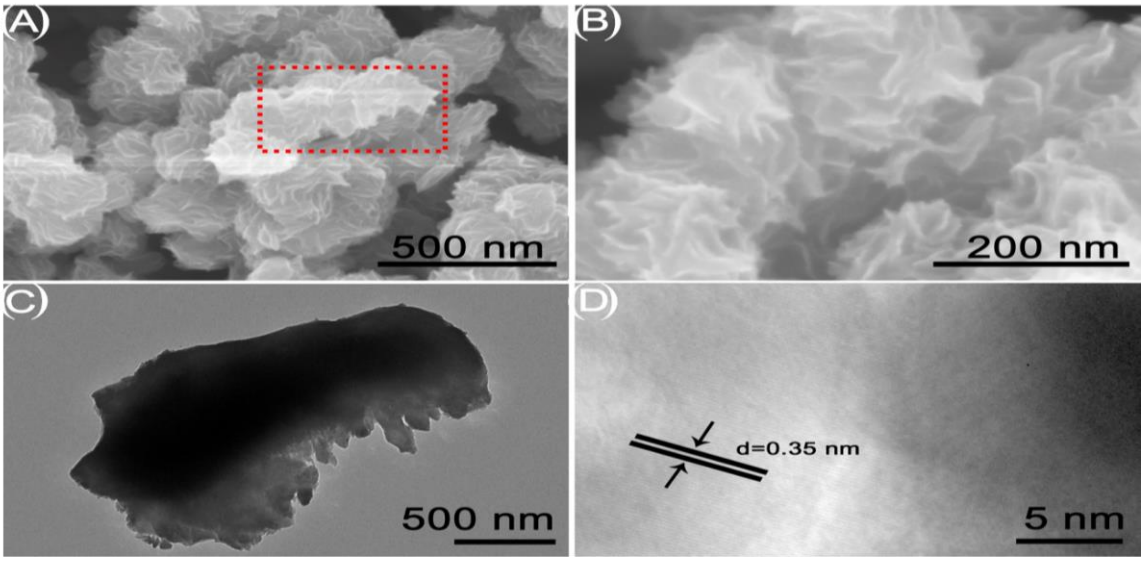

Fig. 2: SEM images of TiO_2-400 (A) and TiO_2-500 (B), TEM image (C) and HRTEM image of TiO_2-500 (D).

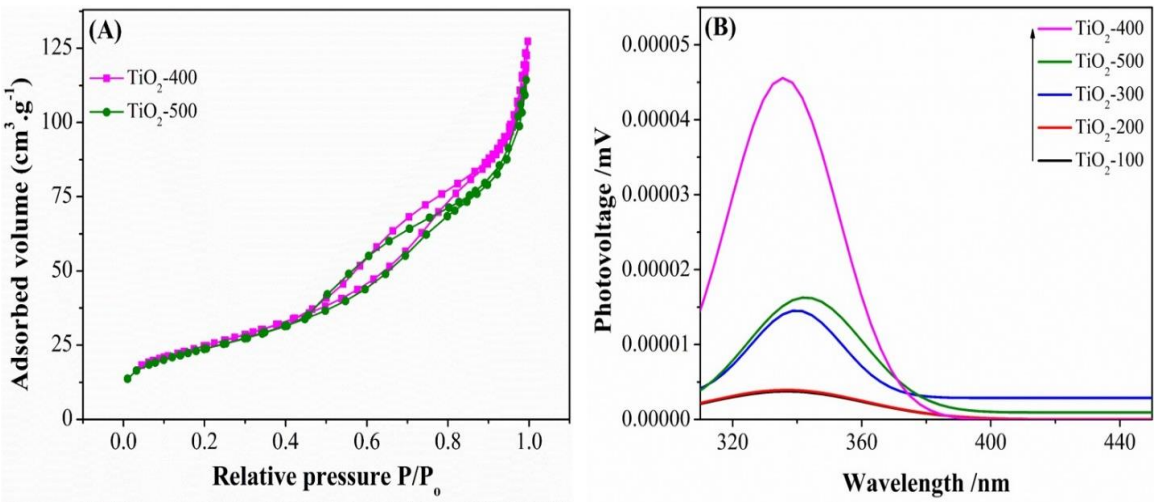

Fig. 3: BET surface area of TiO_2-400 and TiO_2-500 (A) and steady-state surface photovoltage spectra of TiO_2-X (B).

The BET surface areas of TiO_2-400 and TiO_2-500 samples were measured and the results are shown in Fig 3A. It is obvious that the specific surface area of TiO_2-400 sample (87.2517 m²/g) is relatively high than the specific surface area of TiO_2-500 sample (82.9187 m²/g). This high surface area of TiO_2-400 will allow more water molecules to adsorb on its surface for enhanced H_2 evolution.

Charge separation

Charge separation is the most important factor during photocatalysis after the photocatalyst absorbs solar light and generate excited charges in the form of elections and holes. In order to determine the extent of charge separation in the fabricated samples, the steady-state surface photovoltage spectra (SS-SPS) were measured and the results are shown in Fig 3B. It is accepted that the magnitude of SS-SPS peak intensity is related to the charge separation [51-56]. As can be seen, the SS-SPS peak intensities of the samples prepared at 100 and 200 ºC are very low indicating poor charge separation in TiO_2-100 and TiO_2-200 samples. However, the SS-SPS peak intensity is significantly enhanced when temperature is increased and the highest peak intensity is delivered by TiO_2-400 indicating high charge separation in the sample. Interestingly, further increase in temperature causes an obvious reduction in the SS-SPS peak intensity of TiO_2-500 which may be related to the structural defects formed at the higher calcination temperature.

The charge separation experiments were further extended to photoluminescence (PL) study of the samples and the result are shown in Fig 4A. It is widely believed that the PL intensity is linked with the charge recombination capacity of the sample. Higher is the PL peak intensity, higher is charge recombination and vice versa [57-62]. Obviously, the PL intensity of the samples decreases with calcination temperature. Both TiO_2-100 and TiO_2-200 samples deliver highest PL peak intensities indicating highest charge recombination in the given samples. As calcination temperature is increased, the PL intensities are significantly reduced and the lowest PL intensity is shown by TiO_2-400 indicating low charge recombination in the sample. However, further increase in the calcination temperature causes a visible increase in the PL intensity signifying that charge recombination is increased in TiO_2-500 sample which may be related to the structural defects formed at the higher calcination temperature. The high PL peak intensity of TiO_2-100 and TiO_2-200 is due to the fact that the concentration of the charge trapping centre is relatively high at low temperature. As temperature is increased, the crystalinity is improved and the density of charge trapping centre is decreased to improve charge separation for enhanced photocatalytic activity. At 400 C, the PL peak intensity is the lowest indicating higher charge separation in TiO_2-400 sample. However, further increase in calcination temperature results in the agglomeration of particles to decrease size confinement effect and retard charge separation as can be seen in case of TiO_2-500 sample.

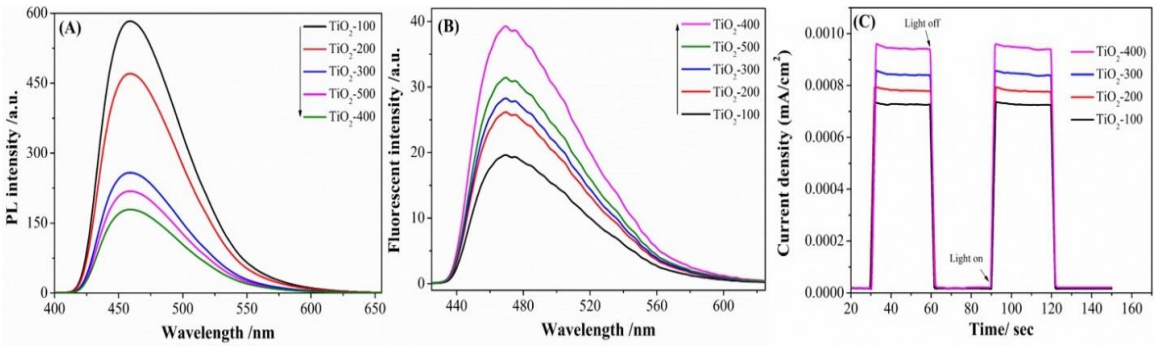

Fig. 4: Photoluminescence spectra (A) fluorescent spectra related to the amount of produced hydroxyl radicals (B) and I-t curves (C) of TiO_2-X.

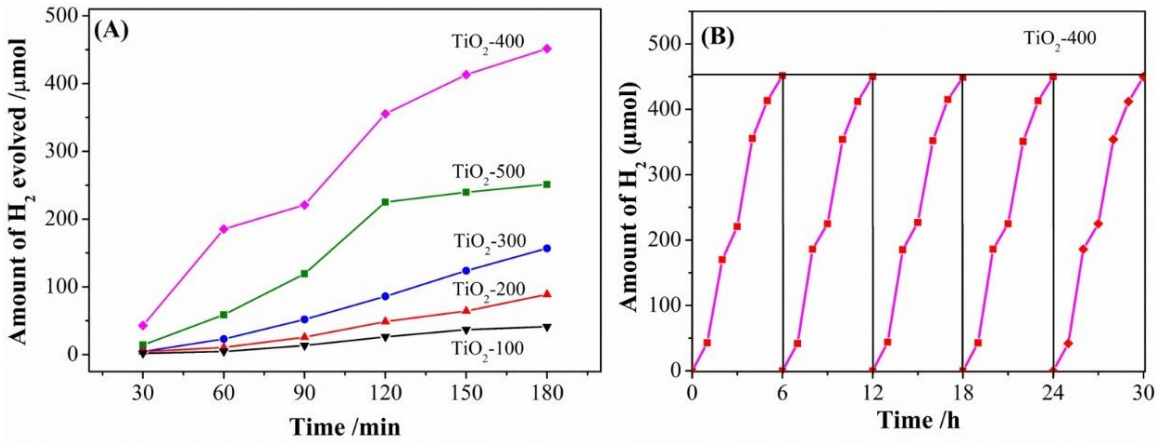

Fig. 5: Photocatalytic activities for H_2 evolution under UV-Visible light (A) and stability test of TiO_2-400 (B).

In order to explain the charge separation in detail, we conducted coumarin based experiments. It is accepted that the hydroxyl radicals produced during photocatalysis react with coumarin to form a luminescent 7-hydroxycoumarin compound, therefore the peak intensity of luminescent 7-hydroxycoumarin gives a clue about the amount of •OH radicals and hence charge separation [63-66]. It is obvious from Fig 4B that the amount of •OH radicals produced by TiO_2-100 and TiO_2-200 is relatively low indicating poor charge separation in the respective compounds. However, the amount of •OH radicals is greatly increased in case of TiO_2-300 and TiO_2-400 samples as expected. Further, the amount of •OH radicals generated by TiO_2-500 sample is slightly low than TiO_2-400 sample which may be related to the poor charge separation as recombination centres are greatly decreased at high temperature.

The charge separation properties were further checked by measuring the electrochemical I-t curves as shown in Fig 4C. Obviously, all the samples show excellent current responses when light is switched on and the current become zero when light is switched off. Interestingly, the sample calcined at 400 ºC shows the highest current response indicating that the photogenerated charges are significantly separated for improved photocatalytic activities.

Photocatalytic water splitting

The photocatalytic activities of the samples were checked by measuring the amount of H_2 gas produced during the photocatalysis of water splitting under UV light irradiation. About 0.1 g sample was vigorously dispersed in a solution containing 80 ml deionized water and 20 ml methanol as hole scavenger in dark for an hour to adsorb water molecules on the surface of the photocatalyst. After that, the suspension was irradiated with a 300 W Xe lamp under UV solar light and the amount of H_2 produced is given in Fig 5A. It is clear that all samples show detectable H_2 generation under the stipulated conditions. The photocatalytic activities of TiO_2-100 and TiO_2-200 are obviously low due to their poor crystalinity and charge separation capacities. However, the generation of H_2

gas is significantly increased as calcination temperature is increased. The highest amount of 451.6 μmol H_2 gas is delivered by TiO_2-400 in 3 h. These photocatalytic activities are consistent with the charge separation experiments. Also the specific surface area of TiO_2-400 is relatively high than TiO_2-500, therefore, TiO_2-400 delivers relatively high photocatalytic activity than TiO_2-500 sample.

We also conducted stability test of TiO_2-400 sample and the results are given in Fig 5B. It is clear that there is no detectable decrease in the H_2 production capability of the sample even after 5 runs in 15 h. This shows that the sample fabricated at 400 C is suitable for H_2 generation for a long time [67-69].

Conclusion

The hydrothermal fabrication of monoclinic TiO_2(B) nanosheets from $TiCl_3$ under different annealing temperature (100, 200, 300, 400 and 500 ^oC) was conducted to optimize the calcination temperature for the preparation of efficient photocatalyst for water splitting under solar light irradiation. The fabricated photocatalyst TiO_2-400 delivered optimum H_2 evolution from water which is attributed to the extended charge separation. The characteristic anisotropic nature of TiO_2(B) plays very crucial role in charge separation as confirmed from the steady-state surface photovoltage spectra, photoluminescence spectra and produced hydroxyl radical amount. It has been concluded that optimum annealing temperature introduces charge trapping centres which help in the separation of excite charges. However, high temperature results in particles aggregation and retards the photocatalytic efficiency.

References

1. R. Taj, E. Pervaiz, A. Hussain, Synthesis and catalytic activity of IM-5 zeolite as naphtha cracking catalyst for light olefins: A review, *J. Chem. Soc. Pak*. **42**, 305 (2020).
2. F. Subhan, S. Aslam, Z. Yan, M. Yaseen, A. Zada, M. Ikram, Fabrication of highly dispersed Pt NPs in nanoconfined spaces of as-made KIT-6 for nitrophenol and MB catalytic reduction in water, *Sep. Purif. Technol*. **265**, 118532 (2021).
3. R. Nazir, M. Khan, R. U. Rehman, S. Shujah, M. Khan, M. Ullah, A. Zada, N. Mahmood, I. Ahmad, Adsorption of selected azo dyes from an aqueous solution by activated carbon derived from Monotheca buxifolia waste seeds, *Soil Water Res*. **15**, 166 (2020).
4. A. Zada, P. Muhammad, W. Ahmad, Z. Hussain, S. Ali, M. Khan, Q. Khan, M. Maqbool, Surface plasmonic-assisted photocatalysis and optoelectronic devices with noble metal nanocrystals: design, synthesis, and applications, *Adv. Funct. Mater*. **30**, 1906744 (2020).
5. F. Ahmadzadeh, B. Karami, M. Farahi and J. Etemad, A novel magnetic nanocatalyst Fe_3O_4@TiO_2-H_5IO_6 for the green synthesis of 4-substituted-1,5-benzodiazepine derivatives, *J. Chem. Soc. Pak*. **43**, 456 (2021).
6. Z. Hussain, A. Zada, K. Hussain, M. Y. Naz, N. M. A. Salam, K. A. Ibrahim, Preparation of activated porous glass adsorbent through thermochemical reforming of ampoules and eggshells for remediation of direct blue dye pollution, *Asia-Pacific J. Chem. Eng*. **16**, e2610 (2021).
7. A. Zada, Y. Qu, S. Ali, N. Sun, H. Lu, R. Yan, X. Zhang, L. Jing, Improved visible-light activities for degrading pollutants on TiO_2/g-C_3N_4 nanocomposites by decorating SPR Au nanoparticles and 2,4-dichlorophenol decomposition path, *J. Hazard. Mater*. **342**, 715 (2018).
8. K. Qi, S. Liu, A. Zada, Graphitic carbon nitride, a polymer photocatalyst, *J. Taiwan Inst. Chem. Eng*. **109** 111 (2020).
9. M. Ullah, R. Nazir, M. Khan, W. Khan, M. Shah, S. G. Afridi, A. Zada, The effective removal of heavy metals from water by activated carbon adsorbents of Albizia lebbeck and Melia azedarach seed shells, *Soil Water Res*. **15** 30-37 (2020).
10. S. S. Madani, A. H. Yangjeh, S. A. Khaneghah, H. Chand, V. Krishnan, A. Zada, Integration of $Bi_4O_5I_2$ nanoparticles with ZnO: Impressive visible-light-induced systems for elimination of aqueous contaminants, *J. Taiwan Inst. Chem. Eng*. **119**, 177 (2021).
11. M. M. Baig, E. Pervaiz, Muhammad J. Afzal, Catalytic activity and kinetic studies of core@shell nanostructure $NiFe_2O_4$@TiO_2 for photocatalytic degradation of methyl orange dye, *J. Chem. Soc. Pak*. **42**, 531 (2020).
12. M. He, J. Zhang, F. Chen, K. Shu, Y. Tang, One-pot fabrication of K-doped g-C_3N_4/SiO_2 composite with enhanced photocatalytic activity for degradation of tetracycline, *J. Chem. Soc. Pak*. **43**, 124 (2021).
13. Z. Zafar, S. Yi, J. Li, C. Li, Y. Zhu, A. Zada, W. Yao, Z. Liu, X. Yue, Recent development in defects engineered photocatalysts: an overview of the experimental and theoretical strategies, *Energy Environ. Mater*. **5** 68-114 (2021).
14. G. Wang, X. Zhao and S. Han, Effect of MgO addition on the properties of Ni/Al2O3 and its catalytic activity in hydrogenation of N-(2`,3`-dimethoxy benzyl)-3,4-dioxy-methylene-

phenylethylamine, *J. Chem. Soc. Pak*. **41**, 796 (2019).

15. N. Ali, Awais, T. Kamal, Mazhar Ul-Islam, A. Khan, S. J. Shah, A. Zada, Chitosan-coated cotton cloth supported copper nanoparticles for toxic dye reduction, *Int. J. Biol. Macromol*. **111**, 832 (2018).
16. T. Ilyas, F. Raziq, N. Ilyas, L. Yang, S. Alia, A. Zada, S. H. Bakhtiar, Y. Wang, H. Shen, L. Qiao, FeNi@CNS nanocomposite as an efficient electrochemical catalyst for N_2-to-NH_3 conversion under ambient conditions, *J. Mater. Sci. Technol.* **103**, 59 (2022).
17. T. Ilyas, F. Raziq, S. Ali, A. Zada, N. Ilyas, R. Shah, Y. Wang, L. Qiao, Facile synthesis of MoS_2/Cu as trifunctional catalyst for electrochemical overall water splitting and photocatalytic CO_2 conversion, *Mater. Des*. **204,** 109674 (2021).
18. M. Khan, A. Hayat, S. K. B. Mane, T. Li, N. Shaishta, D. Alei, T. K. Zhao, A. Ullah, A. Zada, A. U. Rehman, W. U. Khan, Functionalized nano diamond composites for photocatalytic hydrogen evolution and effective pollutant degradation, *Int. J. Hydrogen Energy*, **45,** 29070 (2020).
19. K. Qi, X. Xing, A. Zada, M. Li, Q. Wang, S. Liu, H. Lin, G. Wang, Transition metal doped ZnO nanoparticles with enhanced photocatalytic and antibacterial performances: Experimental and DFT studies, *Ceram. Int.* **46**, 1494 (2020).
20. J. Wang, C. Qin, H. Wang, M. Chu, A. Zada, X. Zhang, J. Li, F. Raziq, Y. Qu, L. Jing, Exceptional photocatalytic activities for CO_2 conversion on Al-O bridged g-C_3N_4/α-Fe_2O_3 Z-scheme nanocomposites and mechanism insight with isotopes, *Appl. Catal. B: Environ*. **221**, 459 (2018).
21. Me. Tezcan, H. Cicek, M. Cicek and S. Nadeem, Tuning photocatalytic activity and decomposition properties of poly(polyethylene glycol diacrylate-co-hydroxyethyl methacrylate)/TiO_2 composite hydrogel, *J. Chem. Soc. Pak*. **41**, 598 (2019).
22. A. Zada, Muhammad Humayun, F. Raziq, X. Zhang, Y. Qu, L. Bai, C. Qin, L. Jing, H. Fu, Exceptional visible-light-driven cocatalyst-free photocatalytic activity of g-C_3N_4 by well-designed nanocomposites with plasmonic Au and SnO_2, *Adv. Energy Mater*. **6,** 1601190 (2016).
23. S. Ali, M. Rahim, P. Fazil, M. S. Ahmad, A. Ullah, M. R. Shah, G. Rukh, M. Ateeq, R. Khattak, M. S. Khan, Synthesis and photonics applications of afzelechin conjugated silver nanoparticles, *Coatings*. **11**, 1295 (2021).
24. A. Zada, M. Khan, M. A. Khan, Q. Khan, A. H. Yangjeh, A. Dang, M. Maqbool, Review on the hazardous applications and photodegradation mechanisms of chlorophenols over different photocatalysts, *Environ. Res*. **195**, 110742 (2021).
25. A. Zada, M. Khan, Z. Hussain, Muhammad I. A. Shah, M. Ateeq, M. Ullah, N. Ali, S. Shaheen, H. Yasmeen, S. N. A. Shah, A. Dang, Extended visible light driven photocatalytic hydrogen generation by electron induction from g-C_3N_4 nanosheets to ZnO through the proper heterojunction, Z. *Phys. Chem.* https://doi.org/10.1515/zpch-2020-1778 (2021).
26. A. Ullah, P. Fazil, G. Rukh, M. T. Muhammad, M. Rahim, M. Ateeq, R. Khattak, M. S. Khan, O. A. Abu Ali, D. I. Saleh, A novel colorimetric chemosensor based on ferene-s-conjugated silver nanoparticles for selective recognition of Fe2+, *Coatings*. **11**, 1293 (2021).
27. K. Saeed, I. Khan, M. Ahad, T. Shah, M. Sadiq, A. Zada, N. Zada, Preparation of ZnO/Nylon 6/6 nanocomposites, their characterization and application in dye decolorization, *Appl. Water Sci.* **11**, 105 (2021).
28. C. Liu, F. Raziq, Z. Li, Y. Qu, A. Zada, L. Jing, Synthesis of Ti_{O2}/g-$_{C3N4}$ nanocomposites with phosphate-oxygen functional bridges for improved photocatalytic activity, *Chin. J. Catal*. **38**, 1072 (2017).
29. S. Ali, Z. Li, S. Chen, A. Zada, I. Khan, I. Khan, W. Ali, S. Shaheen, Y. Qu, L. Jing, Synthesis of activated carbon-supported TiO_2-based nano-photocatalysts with well recycling for efficiently degrading high-concentration pollutants, *Catal. Today*, **335**, 557 (2019).
30. Marchand, R., L. Brohan, and M. Tournoux, TiO2 (B) a new form of titanium dioxide and the potassium octatitanate K2Ti8O17. *Materials Research Bulletin*, **15,** 1129 (1980).
31. X. Luo, Y. Su, Y. Wang, K. P. Homewood, X. Chen, R. Li and Y. Gao, Remarkably enhanced photocatalytic H2 evolution via construction of Ti0. 5Ru0. 5O2/TiO2 (B)/TiO2 (A) three-phase-junctions. *Applied Surface Science*, **567**, 150837 (2021).
32. Luo, X., et al., Tandem CdS/TiO2 (B) nanosheet photocatalysts for enhanced H2 evolution. *Applied Surface Science*,. **515,** 145970 (2020).
33. Luo, X., et al., Hybrid 0D/2D Ni2P quantum dot loaded TiO2 (B) nanosheet photothermal catalysts for enhanced hydrogen evolution. *Applied Surface Science*,. **505,** 144099 (2020).
34. T. N. Pham, V. K. Hoang Bui, Y. Lee, Recent advances in hierarchical anode designs of TiO_2-B nanostructures for lithium-ion batteries, *Int. J. Energy Res.* **45** 17532-17562 (2021).
35. Y. Zhao, A. Zada, Y. Yang, J. Pan, Y. Wang, Z. Yan, Z. Xu, K. Qi, Photocatalytic removal of antibiotics on g-C3N4 using amorphous CuO as cocatalysts, *Front. Chem.* **9**, 797738 (2021).
36. S. Ahmed, T. Arshad, A. Zada, A. Afzal, M. Khan, A. Hussain, M. Hassan, M. Ali, S. Xu,

Preparation and characterization of a novel sulfonated titanium oxide incorporated chitosan nanocomposite membranes for fuel cell application, *Membranes*. **11**, 450 (2021).

37. X. Wang, H. Wang, Microwave-synthesized TiO_2 nanotube as a durable Li^+-storage electrode material, **5** 9022 (2020).
38. A. Hayat, M. Sohail, M. S. Hamdy, M. A. Amin, S. Alharthi, T. Taha, M. M. Rahman, A. Palamanit, J. Khan, S. K. B. Mane, Biomass lignin integrated polymeric carbon nitride for boosted photocatalytic hydrogen and oxygen evolution reactions, *Mol. Catal*. **518**, 112064 (2022).
39. S. Sabbagh, Mohammad A. Behnajady, Synthesis of TiO_2 (B) and high-temperature stable anatase TiO_2 nanowires by hydrothermal method and investigation of photocatalytic activity, *Photochem. Photobiol*. **95** 733 (2019).
40. M. Khan, L. Tiehu, S. B. A. Zaidi, E. Javed, A. Hussain, A. Hayat, A. Zada, D. Alei, A. Ullah, Synergistic effect of nanodiamond and titanium oxide nanoparticles on the mechanical, thermal and electrical properties of pitch-derived carbon foam composites, *Polym. Int.* **70**, 1733 (2021).
41. A. Zada, M. Khan, Z. Hussain, M. I. A. Shah, M. Ateeq, M. Ullah, N. Ali, S. Shaheen, H. Yasmeen, S. N. A. Shah, Extended visible light driven photocatalytic hydrogen generation by electron induction from g-C3N4 nanosheets to ZnO through the proper heterojunction, *Z. Phys. Chem.* **236**, 53 (2022).`
42. Z. Hussain, G. Rukh, A. Zada, M. Naz, K. Khan, S. Shukrullah, S. Sulaiman, Construction of rechargeable bio-battery cells from electroactive antioxidants extracted from wasted vegetables, *Cleaner Eng. Technol.* **5**, 100342 (2021).
43. Md. K. Hossain, A. R. Koirala, U. S. Akhtar, M. K. Song, K. B. Yoon, First synthesis of highly crystalline hexagonally ordered uniformly mesoporous TiO_2-B and its optical and photocatalytic properties, *Chem. Mater*. **27**, 6550 (2015).
44. F. Raziq, A. Aligayev, H. Shen, S. Ali, R. Shah, S. Ali, S. H. Bakhtiar, A. Ali, N. Zarshad, A. Zada, X. Xia, X. Zu, M. Khan, X. Wu, Q. Kong, C. Liu, L. Qiao, Exceptional photocatalytic activities of rGO modified (B, N) co-doped WO_3, coupled with CdSe QDs for one photon Z-scheme system: A joint experimental and DFT study, *Adv. Sci*. **9** 2102530 (2021).
45. L. Wu, X. Yang, J. Li, Y. Huang, X. Li, Fabrication of titanium dioxide nanotubes with good morphology at high calcination temperature and their photocatalytic activity, *Mater. Chem. Phys.* **202** 136-142 (2017).
46. K. Qi, A. Zada, Y. Yang, Q. Chen, A. Khataee, Design of 2D-2D NiO/g-$_{C3N4}$ heterojunction photocatalysts for degradation of an emerging pollutant, *Res. Chem. Intermed*. **46**, 5281 (2020).
47. W. Ali, H. Ullah, A. Zada, M. K. Alamgir, W. Muhammad, M. J. Ahmad, A. Nadhman, Effect of calcination temperature on the photoactivities of ZnO/SnO_2 nanocomposites for the degradation of methyl orange, *Mater. Chem. Phys*. **213**, 259 (2018).
48. Z. Zhang, A. Zada, N. Cui, Naiwen Liu, M. Liu, Y. Yang, D. Jiang, J. Jiang, S. Liu, Synthesis of Ag loaded ZnO/BiOCl with high photocatalytic performance for the removal of antibiotic pollutants, *Crystals* **11**, 981 (2021).
49. J. Bian, Y. Qu, R. Fazal, X. Li, N. Sun, L. Jing, Accepting excited high-energy-level electrons and catalyzing H2 evolution of dual-functional Ag-TiO2 modifier for promoting visible-light photocatalytic activities of nanosized oxides, *J. Phys. Chem. C* **120**, 11831-11836 (2016) .
50. H. Zhang, S. Sun, H. Ding, T. Deng, J. Wang, Effect of calcination temperature on the structure and properties of SiO2 microspheres/nano-TiO2 composites, *Mater. Sci. Semicond. Process.* **115** 105099 (2020).
51. X. Chu, Y. Qu, A. Zada, L. Bai, Z. Li, F. Yang, L. Zhao, G. Zhang, X. Sun, Z. Yang, L. Jing, Ultrathin phosphate-modulated Co phthalocyanine/g-C_3N_4 heterojunction photocatalysts with single Co-N_4 sites for efficient O_2 activation, *Adv. Sci*. **7**, 2001543 (2020).
52. W. Ali, H. Ullah, A. Zada, W. Muhammad, S. Ali, S. Shaheen, M. K. Alamgir, M. Z. Ansar, Z. Ullah Khan, H. Bilal, P. S. Yap, Synthesis of TiO_2 modified self-assembled honeycomb ZnO/SnO_2 nanocomposites for exceptional photocatalytic degradation of 2,4-dichlorophenol and bisphenol A, *Sci. Total Environ*. **746**, 141291 (2020).
53. B. Xu, A. Zada, G. Wang, Y. Qu, Boosting the visible-light photoactivities of $BiVO_4$ nanoplates by doping Eu and coupling CeO_x nanoparticles for CO_2 reduction and organic oxidation, *Sust. Energy Fuels*, **3**, 3363 (2019).
54. A. Zada, M. Khan, M. N. Qureshi, S. Liu, R. Wang, Accelerating photocatalytic hydrogen production and pollutant degradation by functionalizing g-C_3N_4 with SnO_2, *Front. Chem*. **7**, 941 (2020).
55. S. J. Shah, A. Khan, N. Naz, A. Ismail, Muhammad Zahid, Muhammad S. Khan, Awais, Muhammad Ismail, S. H. Bakhtiar, I. Khan, B. Ahmad, N. Ali, A. Zada, S. Ali, Synthesis of $CoCrFeO_4$-chitosan beads sun-light-driven photocatalyst with well

recycling for efficiently degrading high-concentration dyes, Spectrochim. *Acta Mol. Biomol. Spectrosc*. **236**, 118314 (2020).

56. R. Yan, A. Zada, L. Sun, Z. Li, Z. Mu, S. Chen, F. Yang, J. Sun, L. Bai, Y. Qu, L. Jing, Comparative study of metal oxides and phosphate modification with different mechanisms over g-C_3N_4 for visible-light photocatalytic degradation of metribuzin, *Rare Met.* doi.org/10.1007/s12598-021-01857-3 (2021).
57. H. Yasmeen, A. Zada, S. Liu, Surface plasmon resonance electron channeled through amorphous aluminum oxide bridged ZnO coupled g-C_3N_4 significantly promotes charge separation for pollutants degradation under visible light, *J. Photochem. Photobiol. A: Chem*. **400**, 112681 (2020).
58. H. Yasmeen, A. Zada, S. Liu, Dye loaded MnO_2 and chlorine intercalated g-C_3N_4 coupling impart enhanced visible light photoactivities for pollutants degradation, *J. Photochem. Photobiol. A: Chem*. **380** 111867 (2019).
59. H. Yasmeen, A. Zada, S. Ali, I. Khan, W. Ali, W. Khan, M. Khan, N. Anwar, A. Ali, A. M. H. Flores, F. Subhan, Visible light excited surface plasmon resonance charge transfer significantly improves the photocatalytic activities of ZnO semiconductor for pollutants degradation, *J. Chin. Chem. Soc*. **67**, 1611 (2020).
60. H. Yasmeen, A. Zada, W. Li, M. Xu, S. Liu, Suitable energy platform of Bi_2WO_6 significantly improves visible-light degradation activity of g-C_3N_4 for highly toxic diuron pollutant, *Mater. Sci. Semicond. Process*. **102**, 104598 (2019).
61. M. Xu, A. Zada, R. Yan, H. Li, N. Sun, Y. Qu, Ti_2O_3/TiO_2 heterophase junctions with enhanced charge separation and spatially separated active sites for photocatalytic CO_2 reduction, *Phys. Chem. Chem. Phys*. **22**, 4526 (2020).
62. A. Zada, N. Ali, F. Subhan, N. Anwar, Muhammad I. A. Shah, Muhammad Ateeq, Z. Hussain, K. Zaman, M. Khan, Suitable energy platform significantly improves charge separation of g-C_3N_4 for CO_2 reduction and pollutant oxidation under visible-light, *Prog. Nat. Sci. Mat. Int*. **29**, 138 (2019).
63. A. Zada, N. Ali, M. Ateeq, A. M. H. Flores, Z. Hussain, S. Shaheen, M. Ullah, S. Ali, I. Khan, W. Ali, Muhammad I. A. Shah, W. Khan, Surface plasmon resonance excited electron induction greatly extends H_2 evolution and pollutant degradation activity of g-C_3N_4 under visible light irradiation, *J. Chin. Chem. Soc*. **67**, 983 (2020).
64. N. Ali, A. Zada, M. Zahid, A. Ismail, M. Rafiq, A. Riaz, A. Khan, Enhanced photodegradation of methylene blue with alkaline and transition-metal ferrite nanophotocatalysts under direct sun light irradiation, *J. Chin. Chem. Soc*. **66**, 402 (2019).
65. J. Wu, H. Lu, X. Zhang, F. Raziq, Y. Qu, L. Jing, Enhanced charge separation of rutile TiO_2 nanorods by trapping holes and transferring electrons for efficient cocatalyst-free photocatalytic conversion of CO_2 to fuels, *Chem. Commun*. **52**, 5027 (2016).
66. J. Li, X. Zhang, F. Raziq, J. Wang, C. Liu, Y. Liu, J. Sun, R. Yan, B. Qu, C. Qin, L. Jing, Improved photocatalytic activities of g-C_3N_4 nanosheets by effectively trapping holes with halogen-induced surface polarization and 2, 4-dichlorophenol decomposition mechanism, *Appl. Catal. B: Environ*. **218**, 60 (2017).
67. A. Hamid, M. Khan, A. Hayat, J. Raza, A. Zada, A. Ullah, F. Raziq, T. Li, F. Hussain, Probing the physio-chemical appraisal of green synthesized PbO nanoparticles in PbO-PVC nanocomposite polymer membranes, *Spectrochim. Acta Mol. Biomol. Spectrosc*. **235**, 118303 (2020).
68. M. Khan, A. Zada, A. Hayat, T. Ali , I. Uddin, A. Hayat, M. Khan, A. Ullah, A. Hussain, T. Li, T. Zhao, A concise review on the elastomeric behavior of electroactive polymer materials, *Int. J. Energy Res*. **10**, 14306 (2020).
69. M. Khan, A. Hamid, L. Tiehu, A. Zada, F. Attique, N. Ahmad, A. Ullah, A. Hayat, I. Mahmood, A. Hussain, Y. Khan, I. Ahmad, A. Ali, T. K. Zhao, Surface optimization of detonation nanodiamonds for the enhanced mechanical properties of polymer/nanodiamond composites, *Diamond Relat. Mater*. **107** 107897 (2020).